

Percolation transition in the packing of bidispersed particles on curved surfaces

Andrew M. Mascioli, Christopher J. Burke, and Timothy J. Atherton*

*Department of Physics and Astronomy, Tufts University,
574 Boston Avenue, Medford, Massachusetts 02155, USA*

We study packings of bidispersed spherical particles on a spherical surface. The presence of curvature necessitates defects even for monodispersed particles; bidispersity either leads to a more disordered packing for nearly equal radii, or a higher fill fraction when the smaller particles are accommodated in the interstices of the larger spheres. Variation in the packing fraction is explained by a percolation transition, as chains of defects or scars previously discovered in the monodispersed case grow and eventually disconnect the neighbor graph.

Bidispersed mixtures of hard spheres are an important elementary model of a glass transition[1]: at high temperature and low density they flow freely, while as temperature is reduced they become kinetically arrested and form rigid but highly disordered structures[2]. At zero temperature and stress, a similar *jamming* transition to rigidity occurs as a function of density[3, 4] which in 2D tends to occur around a packing fraction of $\Phi = 0.84$ [5, 6]. Jammed structures exhibit distinctive properties including *isostaticity*: the average number of inter-particle contacts is the minimum number required for mechanical stability[7]. Powerful mathematical tools exist[8] to classify jammed and glassy packings of hard particles according to a hierarchy, depending on where individual particles, groups or boundary deformations can unjam the system[9].

Sphere packings, the high density and zero temperature limit of these processes, have been extensively studied in both 2D and 3D Euclidean space[2, 4, 10, 11] revealing strong dimensional dependence: 2D monodispersed spheres tend to crystallize readily, because the locally dense hexagonal packing fills space; in 3D the locally dense tetrahedral packing cannot fill space, permitting a random close packed structure that is the subject of much debate[12–14]. Even in 2D, however, disorder can be induced in bidispersed systems. Molecular dynamics simulations have shown that there is a transition from order to disorder as the degree of bidispersity is increased[15–18], and statistical models of bidispersed particle packings have been used to predict the local features of disordered bidispersed packings[19, 20]. The degree of order or disorder can be measured by an order parameter such as the hexatic bond orientational order[21].

Crystalline order is geometrically frustrated on curved surfaces[22]: an incompatibility between the preferred hexagonal symmetry of the crystalline packing and the topology of the surface necessitates a minimal number of defects—particles with a number of neighbors other than 6—to accommodate the curvature. For monodispersed particles, the packings are mainly crystalline with a transition between isolated defects for small particle number and chains of defects or *scars* akin to grain boundaries in bulk systems that occur above a critical number of

particles $N_c \approx 110$ and grow with system size[23, 24]. The scars may join in asterisk-like motifs[24] and are aligned by anisotropic curvature[25]. Jammed packings on spheres or *spherical codes* have recently been studied in multiple dimensions [26].

In this Letter, we investigate the packing of bidispersed particles on a spherical surface as a simple model of how glasses interact with curvature. We determine the packing fraction, connectivity and hexatic order parameter as a function of particle number N , fraction of large particles $\chi = N_L/N$ and bidispersity $b = (r_1 - r_2) / (r_1 + r_2)$ where r_1 and r_2 are the radii of the particles and $r_1 \geq r_2$. By identifying topological defects from the neighbor graph we show that variation in these parameters is explained by a percolation transition due to growth and connectivity of the scar network, as well as by the possibility of commensurate local packings.

Simulations—Packings with high coverage fraction were produced using a surface relaxation algorithm: N spherical particles are initially placed using random sequential absorption with their centers of mass on a sphere of radius $R = 1$. Particles are randomly assigned to two categories corresponding to larger and smaller radii respectively. The simulation proceeds by, first, *diffusion sweeps* where, particles are moved in random order some distance drawn from a Gaussian distribution of width $\sigma = 2r_1 \times 10^{-3}$ in a random direction along the surface. Moves that cause overlap are rejected. As the packing becomes dense, an adaptive step size is used to reduce the number of moves rejected due to overlap: $\sigma = 10\langle s \rangle$, where $\langle s \rangle$ is the geometric mean of the separation between each particle and its three nearest neighbors. Secondly, *surface relaxation* moves slowly decrease the radius of the surface by an amount ΔR , where initially $\Delta R = 10^{-5}$. After the surface radius is reduced, particles are projected down onto the nearest point on the surface. After projection, a gradient descent minimization is run on the particles (where the interparticle energy is linear in the amount of overlap) until overlap is undone. If overlap can not be undone, the surface relaxation move is undone and particle positions are reset, and simulation continues with ΔR set to $\Delta R/2$. 20 diffusion sweeps are carried out between each surface relaxation step. The

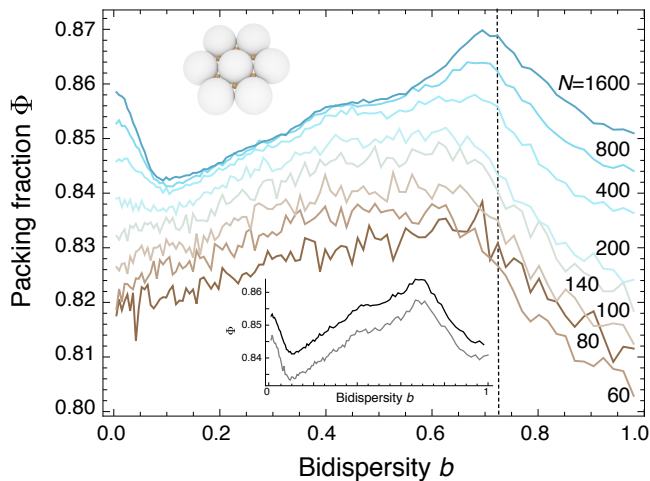


Figure 1. (Color online) Packing fraction Φ as a function of bidispersity $b = (r_1 - r_2) / (r_1 + r_2)$ where $r_1 > r_2$ for different particle numbers N . The maximum $b = \sqrt{3} - 1 \approx 0.73$, indicated with a vertical dashed line, occurs for an Apollonian packing, i.e. where smaller particles fit in the interstices of the larger particles as depicted in the upper inset. Lower inset: comparison of the packing fraction of arrested (gray) and jammed (black) packings for $N = 800$ particles.

simulation halts when ΔR is reduced to 2^{-14} times its original value.

Configurations produced by this procedure are referred to as *arrested*, because they remain metastable if the simulation is restarted; eventually, however, a Monte Carlo move will unjam the arrested configuration, potentially facilitating further relaxation and a consequent increase in the packing fraction. This process occurs in real glasses and is known as *aging*. Extending a powerful technique due to Donev *et al.* [8], we artificially age the arrested structures using a linear program to find and execute an *unjamming* motion of the particles and further relax the surface. Iterative unjamming and relaxation guides the packing toward a state that is collectively jammed with respect to movement of the particles and further relaxation. As we report elsewhere[27], the convergence of this procedure is greatly accelerated by preconditioning the packing, attaching a short range repulsive interaction to the particles beyond the hard inter-penetrability constraint and minimizing the corresponding energy by gradient descent. This procedure moves the particles into the center of the feasible region from which the linear program is more effectively able to identify an unjamming motion. Each arrested structure was subjected to this artificial aging process to produce a corresponding ensemble of *jammed* structures.

For monodispersed particles[23], neighbors are assigned from a Voronoi tessellation[28] of the particle centers of mass, partitioning the surface into N polygonal regions closest to a particular particle. Two particles are neighbors if they share an adjacent edge on

the Voronoi tessellation. Generalizing this construction to bidispersed particles with a weighted distance fails to uniquely assign all points on the surface to a particle; two proposed alternatives [20] are the *radical tessellation* and the *navigation map*, both of which recover the Voronoi tessellation in the limit of monodispersed spheres. The radical tessellation utilizes the radical plane as a separator between each pair of particles; the navigation map partitions the surface into regions closest to the surface of the particles rather than their center of mass. We found little difference between quantities calculated from these constructions and use the radical tessellation exclusively in the remainder of the paper. From the radical tessellation, the adjoint neighbor graph was constructed for each packing and the coordination number determined for each particle.

Results and Discussion—For each value of bidispersity on the interval $b \in [0, 1]$ with a resolution of $\Delta b = 0.005$, an ensemble of 20 jammed configurations was generated with $\chi = 1/2$ and for different numbers of particles N . The packing fraction Φ , i.e. the fraction of the surface enclosed by the particles, was calculated for each configuration and shown in fig. 1. For particle numbers above about $N = 200$, slight deviations from the monodispersed case immediately introduce disorder and reduce the packing fraction as expected. Above a critical value of bidispersity $b_c \sim 0.1$, however, we see a transition and Φ increases, with an apparent shoulder at $b \approx 0.4$, up to a maximum value of $\Phi \approx 0.87$ at $b = b_A \sim 0.7$ and then decreases as $b \rightarrow 1$. For $N < 200$, Φ increases monotonically up to a maximum at a slightly lower value of $b \sim 0.6$. In the lower inset of Fig. 1, we compare the packing fraction for 800 particles for the ensemble of arrested and jammed packings. It is clear that the arrested structures are slightly less efficiently packed, but the trends are identical. We find similar results for all N ; this correspondence affirms that the trends are geometric in origin rather than due to variation in the performance of the algorithm at different b .

The maximum at $b = b_A$ is immediately explicable: it corresponds to the special point at which the smaller particles fit exactly in the interstices between the larger particles, depicted in the upper inset of Fig. 1. We denote this the *Apollonian point* in reference to the tiling. Packings around and above b_A appear mostly crystalline with the smaller particles separated into the interstices; the packing fraction at $b = 1$ corresponds exactly to that for $N/2$ particles. No such immediate explanation is obvious for the low and medium bidispersity results, which appear to be well mixed; we therefore seek a more detailed understanding of the structure.

One structural measure that reflects the degree to which the packings are locally crystalline is the hexatic order parameter $\psi_6 = \langle \exp(i6\theta_i) \rangle$, where the average is taken over the neighboring particles. This is shown calculated from the dataset as a function of b and N in Fig.

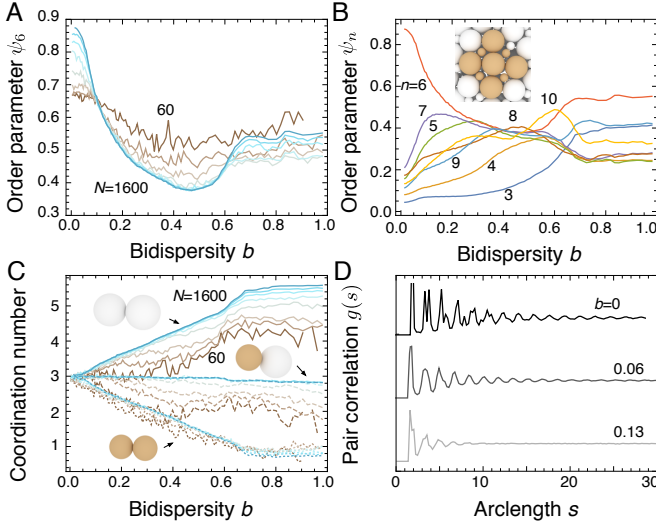


Figure 2. (Color online) **A** Hexatic order parameter as a function of bidispersity b for different N . **B** Local order parameters ψ_n as a function b for a jammed packing of $N = 1600$ particles. Hexatic order dominates except intermediate values of b where eight- and ten-fold order possess maxima. *Inset*: Commensurate configuration with high coordination number at $b = \sqrt{2} - 1 \approx 0.41$. **C** Average coordination number for large-large (solid lines), large-small (dashed lines) and small-small (dotted lines) inter-particle contacts for varying N . **D** Pair correlation function $g(s)$ for three values of bidispersity.

2A. A maximum occurs for all N at $b = 0$ as expected; the value is reduced for smaller N reflecting the disruption of crystallinity by the curvature. The hexatic order drops with b , reaches a minimum around $b \sim 0.45$, rises and then forms a plateau above the Apollonian point, albeit at a value significantly lower than the $b = 0$ case, because here the large particles have a higher coordination number. Variation in ψ_6 is significantly attenuated for low N where the influence of the curvature is stronger.

To see whether hexatic order is replaced by other ordering, we calculated n -atic order parameters $\psi_n = \langle \exp(in\theta_i) \rangle$ for $N = 1600$ as a function of b ; the results are plotted in Fig. 2B. In contrast to the hexatic order parameter, ψ_n for $n \neq 6$ increases with b from $b = 0$; moreover all ψ_n exhibit a plateau above the Apollonian point confirming the distinct nature of this regime. Two values, $n = 8, 10$ have ψ_n narrowly greater than ψ_6 for intermediate values of b and possess maxima at $b = 0.45$ and $b = 0.6$ respectively. Examining the packings, this is due to the presence of octagonally and decagonally coordinated arrangements: a common and commensurate motif, depicted in the inset of fig. 2B, where four large and four small particles are arranged around a central large particle, is allowed first for $b = \sqrt{2} - 1 \approx 0.41$, which coincides with the position of the shoulder in the plot of $\Phi(b)$ in Fig. 1. A variety of similar motifs exist for b around this value with the same coordination number but different mixtures of large and small neighboring

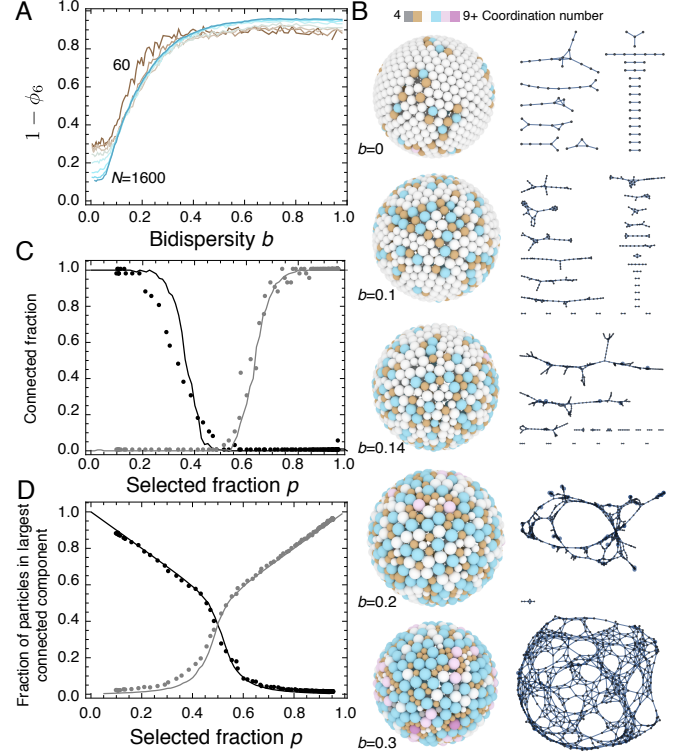


Figure 3. (Color online) **A** Fraction of particles $1 - \phi_6$ with coordination number $C \neq 6$ as a function of bidispersity. **B** Representative defect subgraphs different b illustrating growth and connection of the scar network. **C** Comparison with random percolation: a fraction p sites are randomly selected on a $b = 0$, $N = 800$ neighbor graph. Shown is the fraction of simulations where the selected sites form a connected structure (gray solid line) and the fraction where the non-selected sites retain global connectivity (black solid line). Points show the fraction of simulations where the hexatic (black points) and non-hexatic subgraphs remain connected. **D** Size of the largest connected component for random percolation (solid lines) and bidispersed neighbor graphs (points).

particles and appear to cause the shoulder. It is interesting to note significant decatic ordering: 10-fold rotational symmetry is incompatible with long range order and is rarely seen in packings in flat space with the exception of quasicrystals[29–31]. As long range order is also incompatible with curvature, it appears that curvature may promote the increased 10-fold ordering.

We now examine the coordination number directly. In fig. 2C, we plot the average coordination number per particle, separated into large-large, large-small and small-small contacts and for different N . At infinitesimal b , each particle has six neighbors, three smaller and three larger on average. With increasing b , the number of large-small contacts per particle remains a constant value of three; larger particles gain more large neighbors while smaller particles lose small contacts. At the Apollonian point, the smaller particles are surrounded by three larger neighbors, while the larger particles are on average sur-

rounded by six large neighbors and three smaller neighbors. For $b > b_A$, the coordination numbers remain constant, consistent with the discussion above where smaller particles are caged within the interstices of the larger particles. Smaller values of N follow similar trends, but tend to have lower coordination numbers.

Finally, we calculated the pair correlation function $g(s)$ that encodes particle's local environment; results are displayed in Fig. 2D. For $b = 0$, we see persistent peaks at large s indicative of long range order and a split second peak in agreement with previous studies in flat space[32]. Increasing bidispersity slightly to $b = 0.06$ causes the split peak to disappear, representing the disruption of local crystalline packing, but the long range order persists. Proceeding to $b = 0.13$, $g(s)$ is now flat, indicating that the long range order has disappeared. This is our first indication that the minimum in Φ at b_c observed in Fig. 1 is associated with a transition where long range crystalline order is disrupted.

One measure of the abundance of crystallinity is the fraction ϕ_6 that possess a coordination number of 6. In fig. 3A, we plot $1 - \phi_6$ as a function of bidispersity revealing a transition: as b increases from zero, $1 - \phi_6$ is approximately constant then rises rapidly to unity, reaching a value of $\frac{1}{2}$ at $b = b_p \approx 0.15$. Above bidispersity $b \approx 0.5$, a vanishing fraction of particles possess six neighbors. These trends persist for all values of N shown, but $1 - \phi_6$ is larger at $b = 0$ for small N since topology mandates a minimal number of defects.

To understand this transition further, it is necessary to examine the microstructural information encoded in the neighbor graphs, the adjoint graph of the radical tessellation. We crudely separate the crystalline and non-crystalline components by deleting from a neighbor graph all vertices that have six neighbors, yielding the “non-hexatic” subgraph. Illustrative examples of these subgraphs are depicted in fig. 3B. For $b = 0$ the subgraph consists of small disconnected components corresponding to the previously-studied scars, which are essentially linear in morphology, with a small number of branches. As bidispersity increases to $b = 0.1$, just below b_p , the connected subgraphs are still recognizably scar-like in nature, but have a branching morphology and are substantially longer. By $b = 0.14$, close to b_p , the defect subgraph remains disconnected, but is now dominated by a few large connected graphs that are mostly linear with branches. Finally, above b_p at $b = 0.2$ the defect subgraph is now mostly a single connected structure with a small number of additional isolated defects; it is no longer branching, but with linear sections that link into a foam-like structure. For $b = 0.3$, the defect subgraph retains this structure, but is more densely connected.

The gradual growth and long-range connection of the non-hexatic subgraph due to bidispersity is therefore a percolation transition that occurs: As b increases around b_p , the number of sites participating in the non-hexatic

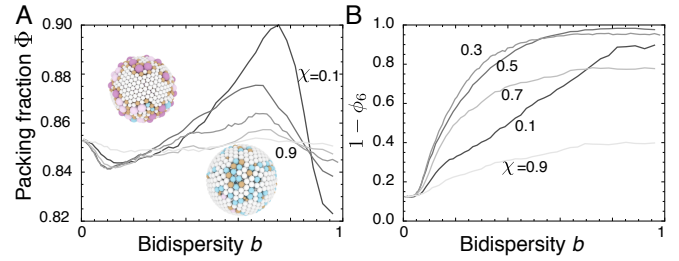


Figure 4. **A** Packing fraction and **B** fraction of particles $1 - \phi_6$ with coordination number $C \neq 6$ as a function of bidispersity for different number fractions of large particles $\chi = N_L/N$. Insets: representative packings shown for $b = 0.33$ and $\chi = 0.1$ (upper) and $\chi = 0.9$ (lower).

subgraph increases until they form a connected structure. Percolation transitions are well-studied[33]. The canonical formulation is: given a network, and selecting a fraction p sites, what is the probability that one of the selected sites belongs to a long-range connected structure? Clearly, the system under consideration cannot be precisely mapped onto this problem because the neighbor graph changes with b . However, by averaging over all particle pairs in Fig. 2B we see that the mean coordination number remains 6 for all b . Thus, we examine the canonical percolation problem on the neighbor graph of a monodisperse packing for $N = 800$ particles. From such a graph, we randomly select a fraction p sites and repeat this procedure to form n trials. Plotted in Fig. 3C is the fraction of trials where the selected components form a connected structure (gray line) and where the remaining components retain their connectivity (black line). We compare this to the bidispersity percolation transition by the placing the non-hexatic subgraph in correspondence to the selected subgraph in the random percolation model; the selected fraction is therefore $p = 1 - \phi_6$. The fraction of connected hexatic and non-hexatic subgraphs at each value of p is plotted as points in Fig. 3C, showing that the percolation thresholds are in good agreement. Notably, the hexatic subgraph become disconnected around $p \approx 0.4$, which occurs at $b \lesssim b_p \approx 0.15$ in Fig. 2A. Percolation implies a growing lengthscale, so we also computed the size of the largest connected component of the selected and unselected subgraphs, plotted in solid lines in Fig. 3D. Again calculating corresponding values from the bidispersed neighbor graphs, shown as points in Fig. 3D, we see excellent agreement. We infer from this that the qualitative features of the bidispersity percolation transition are predicted by a random percolation transition on the monodisperse neighbor graph.

To test this, we attempted to disrupt the transition by varying the fraction of large particles $\chi = N_L/N$, motivated by the idea that growth of the scars might be prevented if sufficiently few minority particles are present. The packing fraction for several values of χ is shown in fig. 4A. Small χ leads to a dramatic enhancement of the

packing fraction at the Apollonian point, but $\chi = 0.9$ flattens it as well as suppresses the low b minimum. Looking at the defect subgraphs, those in $\chi = 0.9$ do not exhibit connected defect subgraphs. For a given χ , bidispersity determines $1 - \phi_6$, which is the parameter that determines whether we have percolation or not: Examining this, plotted in fig. 4B, shows that for $\chi = 0.9$, $1 - \phi_6$ is just short of the threshold ~ 0.4 for random percolation.

Conclusion—We have shown that the packing fraction of bidispersed packings of spheres on a spherical surface is determined by three influences: an Apollonian packing for $b \approx 0.73$ where small particles fit into the interstices of large particles produces a global maximum; commensurate eight and tenfold coordinated configurations of particles yield an inflexion point at $b \approx 0.41$; a minimum at $b \approx 0.1$ is due to the growth and percolation of “scars” previously observed in the monodispersed case. By adjusting the ratio of large particles, we have shown that preventing the percolation transition greatly attenuates the minimum. The growing lengthscale and critical fraction necessary for percolation were found to be in agreement with those for random percolation on the monodispersed neighbor graph.

Acknowledgement—The authors thank the Research Corporation for Science Advancement for funding through a Cottrell Award.

* timothy.atherton@tufts.edu

- [1] F. H. Stillinger and P. G. Debenedetti, *Annu. Rev. Condens. Matter Phys.* **4**, 263 (2013).
- [2] A. Donev, *Journal of Applied Physics* **95**, 989 (2004).
- [3] M. Cates, J. Wittmer, J.-P. Bouchaud, and P. Claudin, *Physical review letters* **81**, 1841 (1998).
- [4] A. J. Liu and S. R. Nagel, *Annual Review of Condensed Matter Physics* **1**, 347 (2010).
- [5] C. O’Hern, S. Langer, A. Liu, and S. Nagel, *Physical Review Letters* **88**, 075507 (2002).
- [6] C. Reichhardt and C. O. Reichhardt, *Soft matter* **10**, 2932 (2014).
- [7] S. Alexander, *Physics Reports* **296**, 65 (1998).
- [8] A. Donev, S. Torquato, F. H. Stillinger, and R. Connelly, *Journal of Computational Physics* **197**, 139 (2004), arXiv:0208502 [cond-mat].
- [9] S. Torquato and F. H. Stillinger, *Journal of Physical Chemistry* **105**, 11849 (2001).
- [10] S. Torquato and F. H. Stillinger, *Reviews of Modern Physics* **82**, 2633 (2010).
- [11] B. Lubachevsky, F. Stillinger, and E. Pinson, *Journal of Statistical Physics* **64**, 501 (1991).
- [12] S. Torquato, T. M. Truskett, and P. G. Debenedetti, *Physical review letters* **84**, 2064 (2000).
- [13] A. Donev, S. Torquato, F. H. Stillinger, and R. Connelly, *Phys. Rev. E* **70**, 043301 (2004).
- [14] R. D. Kamien and A. J. Liu, *Physical review letters* **99**, 155501 (2007).
- [15] T. Hamanaka and A. Onuki, *Physical Review E - Statistical, Nonlinear, and Soft Matter Physics* **74**, 1 (2006), arXiv:0605251 [cond-mat].
- [16] M. R. Sadr-Lahijany, P. Ray, and H. E. Stanley, *Physical Review Letters* **79**, 3206 (1997), arXiv:9705218 [cond-mat].
- [17] W. Vermohlen and N. Ito, **51** (1995).
- [18] H. Watanabe, S. Yukawa, and N. Ito, *Physical Review E - Statistical, Nonlinear, and Soft Matter Physics* **71**, 1 (2005).
- [19] S. Hilgenfeldt, *Philosophical Magazine* **93**, 4018 (2013).
- [20] P. Richard, L. Oger, J. P. Troade, and a. Gervois, *European Physical Journal E* **6**, 295 (2001).
- [21] D. Nelson and B. Halperin, *Physical Review B* **19** (1979).
- [22] H. Seung and D. Nelson, *Physical Review A* **38**, 1005 (1988).
- [23] A. Bausch, M. Bowick, A. Cacciuto, A. Dinsmore, M. Hsu, D. Nelson, M. Nikolaides, A. Travesset, and D. Weitz, *Science (New York, N.Y.)* **299**, 1716 (2003).
- [24] M. Bowick, D. Nelson, and A. Travesset, *Physical Review B* **62**, 8738 (2000).
- [25] C. J. Burke, B. L. Mbanga, Z. Wei, P. Spicer, and T. Atherton, *Soft Matter* (2015), 10.1039/C5SM01118C.
- [26] H. Cohn, Y. Jiao, A. Kumar, and S. Torquato, *Geometry & Topology* **15**, 2235 (2011).
- [27] C. J. Burke and T. J. Atherton, submitted, arXiv:1605.09478 (2016).
- [28] F. Aurenhammer, *ACM Computing Surveys (CSUR)* **23**, 345 (1991).
- [29] D. Shechtman, I. Blech, D. Gratias, and J. W. Cahn, *Phys. Rev. Lett.* **53**, 1951 (1984).
- [30] S. Fischer, A. Exner, K. Zielske, J. Perlich, S. Deloudi, W. Steurer, P. Lindner, and S. Färster, *Proceedings of the National Academy of Sciences* **108**, 1810 (2011).
- [31] D. V. Talapin, E. V. Shevchenko, M. I. Bodnarchuk, X. Ye, J. Chen, and C. B. Murray, *Nature* **461**, 964 (2009).
- [32] A. Donev, S. Torquato, and F. Stillinger, *Physical Review E* **71**, 011105 (2005).
- [33] G. Grimmett, in *Lectures on Probability Theory and Statistics* (Springer, 1997) pp. 153–300.